$$\nabla \times \left(\frac{1}{\mu_r}\nabla \times \boldsymbol{E}\right) - k_0^2 \varepsilon_r \boldsymbol{E} = 0$$

Hybrid Triangulated Convex Serrated MSP Antenna Analysis Using FEM Technique

G. Asa Jyothi [1], B. Prabhakar Rao [2]
[1] Associate Professor, Department of ECM, K L University, asajyothi.2012@kluniversity.in
[2] Director, Admissions, JNTUK, Kakinada

Abstract— The objective of antenna analysis is to predict the radiation characteristics such as radiation patterns, gain and polarization as well as near fields' characteristics such as Input impedance, bandwidth, mutual coupling and antenna efficiency. Many elaborate techniques have been used to determine micro strip antenna characteristics. In the current paper FEM technique was used which is more efficient for finite size antennas to analyze the characteristics of hybrid triangulated convex serrated micro strip antenna. Serrations are implemented to the radiator to make the antenna use for multiple applications and to improve the performance due to reduction of edge diffractions. Most of important antenna parameters like Return loss, input impedance ,Radiation fields in E and H planes, maximum gain etc. are analyzed using HFSS 13 Simulator.

Index Terms— FEM techniques, Hybrid Serrations, Edge Diffractions

1 INTRODUCTION:

The idea of micro strip patch antenna arose from utilizing printed circuit technology, not only for the circuit components and transmission lines but also for the radiating elements of an electronic system. The basic structure of the micro strip antenna consists of an area of metallization supported above a ground plane by a thin dielectric substrate and fed against the ground at an appropriate location. The patch shape can in principle be arbitrary; in practice, the rectangle, the circle, the equi triangle and the annular-ring are common shapes. In the current paper, rectangular patch is designed along with hybrid triangulated convex serrations. Serrations are introduced on the patch of the antenna to make it operated for multiband applications and to reduce the effect of edge diffractions from the surface of the patch aperture.

By analyzing the antenna parameters, it is possible to predict the radiation patterns, gain, polarization, input impedance, impedance bandwidth, mutual coupling and antenna efficiency. Many techniques have been used include the transmissions line model, generalized transmission line model, cavity model and multiport network model. These techniques are simple but not accurate due to the basic geometry of the micro strip antenna. The simulation technique used to calculate the three dimensional electromagnetic field inside a structure is based on the finite element method (FEM). The principle of the method is to divide the study area into many small regions (tetrahedrons), then calculate the local electromagnetic field in each element. Any embedded semiconductor device in the antenna can be included in the analysis at the device-filed interaction level. This possibility leads to an accurate analysis of active micro strip antenna.

2 THE MATHEMATICAL METHOD

In the current work, a numerical technique called the Finite Element Method (FEM) is used to measure the field components. In this method, the antenna radiating structure is subdivided into many smaller subsections called finite elements. The finite elements used are named as tetrahedra, and the entire collection of tetrahedra is called a mesh. A solution is found for the fields within the finite elements, and these fields are interrelated so that Maxwell's equations are satisfied across inter-element boundaries. Yielding a field solution for the entire, original, structure. Once the field solution has been found, the generalized S-matrix solution is determined.

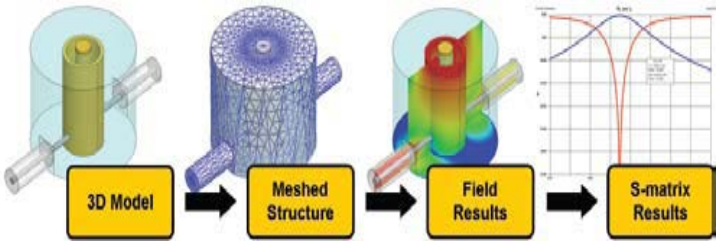

Fig 1. Block diagram of process of analysis of MSP Antenna.

Mathematically, The local fields and are calculated in each tetrahedron from the following eqs.(1) and (2), subject to excitations and boundary conditions[5][6].

…(1)

Where

$$\mu_r = \frac{\mu}{\mu_0}, \varepsilon_r = \frac{\varepsilon}{\varepsilon_0}, k_0^2 = \omega^2 \varepsilon_0 \mu_0 = \frac{\omega^2}{c^2}$$

The magnetic field ***H*** is calculated using equation (2),

$$H = \frac{1}{w\mu} \nabla X E \quad \ldots(2)$$

The remaining electromagnetic quantities are derived using the constitutive relations. Here, The interpolation method is used combined with an iterative process in which a mesh is created automatically and redefined in the critical regions. The simulator generates a solution based on the predefined initial mesh. Then, it refines the mesh in regions where there is a high density of errors, and generates a new solution.

1. Divide the structure into a finite element mesh using tetrahedral elements.
2. Define testing functions *Wn*, for each tetrahedron, resulting in thousands of basis functions
3. Multiply field equation (1) by a *Wn* and integrate over the solution volume

… (3)

This procedure yields thousands of equations for *n*=1, 2,…,*N*
Manipulating the N equations, using Green's theorem and the divergence theorem which yields

$$\sum x_m \int_V \left[(\nabla \times W_n) \cdot \left(\frac{1}{\mu_r} \nabla \times W_m \right) - k_0^2 W_n \cdot W_m \right] dV = \int_S (boundary\ terms)\, dS$$

…(3.a)

for *n*=1,2,…,*N* writing,

… (4)

rewrites (3a) as,

$$\sum x_m \int_V \left[(\nabla \times W_n) \cdot \left(\frac{1}{\mu_r} \nabla \times W_m \right) - k_0^2 W_n \cdot W_m \right] dV = \int_S (boundary\ terms)\, dS$$

… (5)

for *n*=1,2,…,*N*
Equation (5) then has the form

$\sum x_m A_{n,m} = b_n$, n = 1,2,3,……. N. … (6)

Or Ax = b… (7)

In the matrix equation, *A* is a known NxN matrix that includes any applied boundary condition terms, while *b* contains the port excitations, voltage and current sources and incident waves. Once solving for *x*, from eq.(7) ,it is possible to obtain the ***E***.

The field solution process used is iterative process. It ie required to use the above process repeatedly, changing the mesh in a very deliberate manner, until the correct field solution is found. This repetitive process is known as the adaptive iterative solution process and is a key to the highly accurate results.

3. THE ADAPTIVE SOLUTION PROCESS AND ITS IMPORTANCE TO HFSS

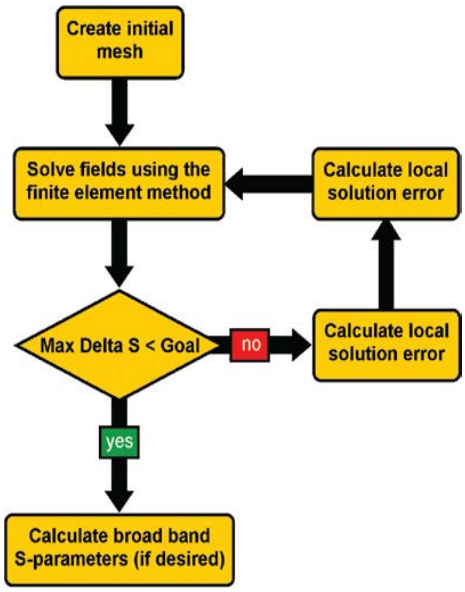

Fig.2. Block Representation of Adaptive Process

The adaptive analysis is a solution process in which the mesh is refined iteratively. Refinement of the mesh is localized to regions where the electric field solution error is high. This adaptive refinement increases the solution's accuracy with each adaptive solution.

Following is the general process followed during an adaptive analysis:

1. First generate an initial, geometrically conformal, mesh.
2. Using the initial mesh, the electromagnetic fields that exist inside the structure are computed when it is excited at the solution frequency.
3. A pre-defined percentage of tetrahedras in these regions are refined. Tetrahedra are refined by creating a number of smaller tetrahedra that replace the original larger element.
4. Then another solution is obtained using the refined mesh.
5. This iterative process (solve -> error analysis -> refine) repeats until the convergence criteria are satisfied or the requested number of adaptive passes is completed.
6. The above process will create a geometrically conformal, and electromagnetically appropriate mesh which ensures correct result to a given simulation.

Mathematically, the error is computed along the following lines. Let E*approx* be the solution to step 2. above. This value is inserted back into eq.(8

… (8)

yielding

$$\nabla \times \left(\frac{1}{\mu_r} \nabla \times E \right) - k_0^2 \varepsilon_r E = 0$$

$$\nabla \times \left(\frac{1}{\mu_r}\nabla \times E^{approx}\right) - k_0^2 \varepsilon_r E^{approx} = residue \quad \ldots (9)$$

For each tetrahedron in the mesh, the residue function is evaluated. A percentage of the tetrahedra with high residue values are selected and refined.

3 Design of Serrations:

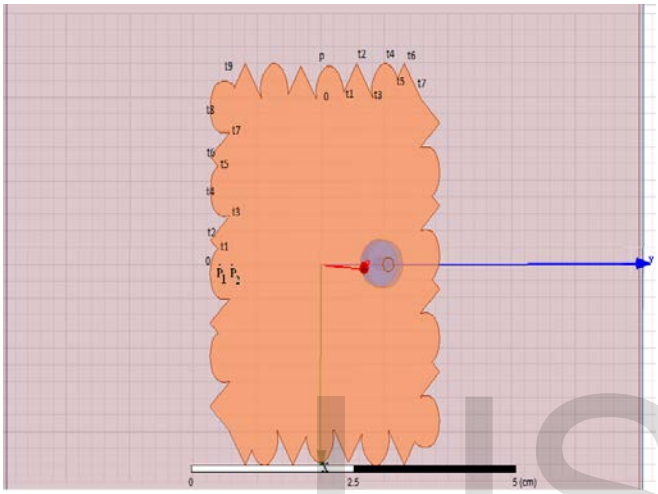

Fig 3.a: Model 1 MSP Antenna

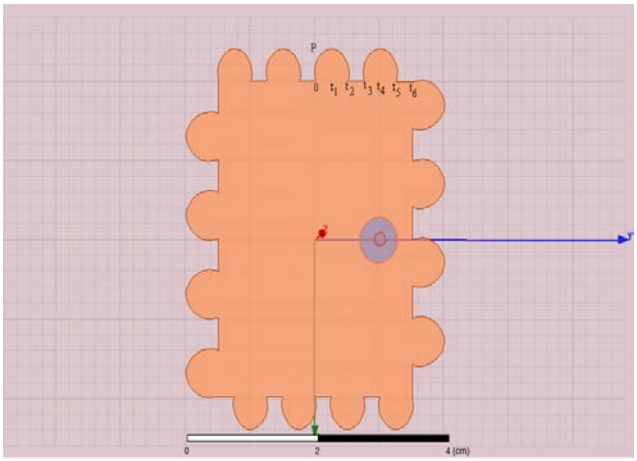

Fig 3.b: Model 2 MSP Antenna

In model1 as shown in fig. 3.a, Triangulated convex serrations are designed along the x-axis of the Microstrip patch aperture of dimensions (3.97 X 3) cm with each serration of size 0.992 cm. The serrations on the x-axis are represented with the below equations.

$$f(x') = (p_2 - p_1)e^{(-at_1)} + (p_2 - p_1)\left(1 - e^{(-a(t_1 - x)}\right) \quad for \quad 0 \le x' < t_1$$

$$= \frac{(p_2 - p_1)(x' - t_1)}{t_2 - t_1} \qquad t_1 \le x' < t_2$$

$$= \frac{(-p_2)(x' - t_3)}{t_3 - t_2} \qquad t_2 \le x' < t_3$$

$$= p_2\left(e^{(-a(t_4 - t_3)}\right) + p_2\left(1 - e^{(-a(x' - t_3)}\right) \text{ for } \quad t_3 \le x' < t_4$$

$$= (p_2 - p_1)\left(e^{(-a(t_5 - t_4)}\right) + (p_2 - p_1)\left(1 - e^{(-a(t_5 - x')}\right) \qquad t_4 \le x' < t_5$$

$$= \frac{(p_2 - p_1)(x' - t_5)}{t_6 - t_5} \qquad t_5 \le x' < t_6$$

$$= \frac{(-p_2)(x' - t_7)}{t_7 - t_6} \qquad t_6 \le x' < t_7$$

$$= p_2\left(e^{(-a(t_8 - t_7)}\right) + p_2\left(1 - e^{(-a(x' - t_7)}\right) \qquad t_7 \le x' < t_8$$

$$= p_2\left(e^{(-a(t_9 - t_8)}\right) + p_2\left(1 - e^{(-a(t_9 - x')}\right) \qquad t_8 < x' < t_9$$

The Hydrid convex and triangle serrations along the y-axis of model 1 MSP antenna as in Fig.3.a are represented by the following equations.

$$f(y') = p_2 e^{(-at_1)} + \quad p_2\left(1 - e^{(-a(t_1 - y')}\right) \quad for \quad 0 < y' < t_1$$

$$= \frac{(p_2)(y' - t_1)}{t_2 - t_1} \qquad t_1 < y' < t_2$$

$$= \frac{(-p_2)(y' - t_3)}{t_3 - t_2} \qquad t_2 < y' < t_3$$

$$= p_2\left(e^{(-a(t_4 - t_3)}\right) + p_2\left(1 - e^{(-a(y' - t_3)}\right) \text{ for } t_3 < y' < t_4$$

$$= (p_2)\left(e^{(-a(t_5 - t_4)}\right) + (p_2)\left(1 - e^{(-a(t_5 - y')}\right) \; t_4 < y' < t_5$$

$$= \frac{(p_2)(y' - t_5)}{t_6 - t_5} \qquad t_5 < y' < t_6$$

$$= \frac{(-p_2)(y' - t_7)}{t_7 - t_6} \qquad t_6 < y' < t_7$$

Fig 3.b illustrates the rectangular aperture patch antenna (3.97 X 3) cm of model 2 employing the variable convex serrations of widths 0.585 cm and 0.5 cm on the x and y axis respectively. The elements spacing on both x and y-axis are 0.41 cm and 0.25 cm respectively. The serration functions on x-axis are defined as follows --

$$f(x') = pe^{(-at_1)} + \left(1 - e^{(-a(t_1 - x')}\right) \qquad for \quad 0 < x' < t_1$$

$$= pe^{(-a(t_2 - t_1)} + \left(1 - e^{-(-a(t_1 - x')}\right) \qquad t_1 < x' < t_2$$

$$= 0 \qquad t_2 < x' < t_3$$

$$= pe^{(-a(t_4-t_3)} + p\left(1 - e^{-(-a(x'-t_3)}\right) \qquad t_3 < x' < t_4$$

$$= pe^{(-a(t_5-t_4)} + p\left(1 - e^{-(-a(t_5-x')}\right) \qquad t_4 < x' < t_5$$

$$=0 \qquad t_5 < x' < t_6$$

4 .Analysis of Result

The various MSP antenna parameters are obtained by using HFSS 13 simulator. With hybrid triangulated convex serrations as in fig.3.a, the MSP antenna resonates at dual frequencies 2.57 GHz and 4.07 GHz with a return loss of -22.18dB and -16.02dB respectively. The various resultant parameters of the model 1 MSP antenna are as shown in figs. 4. The impedance matching at input coaxial feed terminals is occurred at 86 ohms. It gives maximum gain of 7.07db with E & H-fields radiation intensity of 5.39v/m and 5.33 v/m respectively. It provides reasonably good surface current density radiation of 6.14A/m, which are sufficient for most of the commercial communication applications in S band region. The resultant characteristic waveforms are as shown in fig.4.

The performance of the variable width convex serrated MSP antenna as shown in fig.3.b is analyzed with respect to its results shown in figs.5. It also resonated as dual band antenna at frequencies 2.45GHz and 3.95GHz with good return loss of -18.22dB & -16.95dB.The input impedance of this antenna design is 84 ohms with the maximum gain of 6.24dB and 12dB in directions of θ *and* $\emptyset$. The radiation intensity of E-field, H-field and J-field are 3.32v/m, 2.28v/m and 3.18v/m respectively.

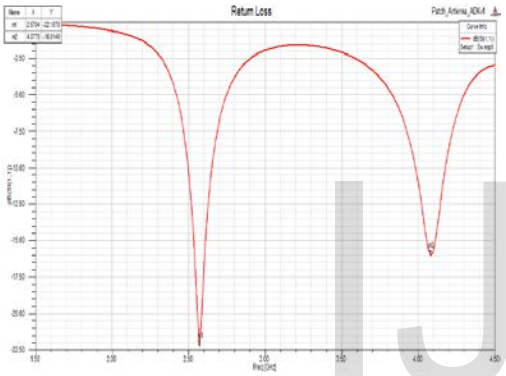

Fig 4.a: Return Loss of Model 1 Antenna

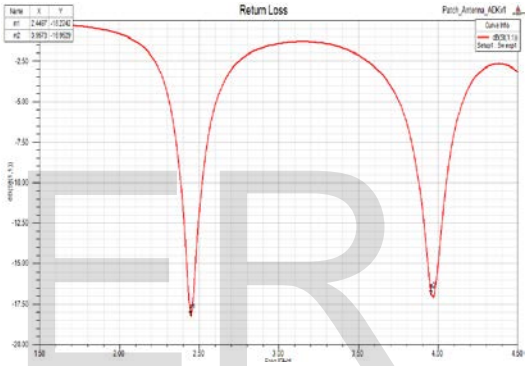

Fig 5.a: Return Loss of Model 2 Antenna

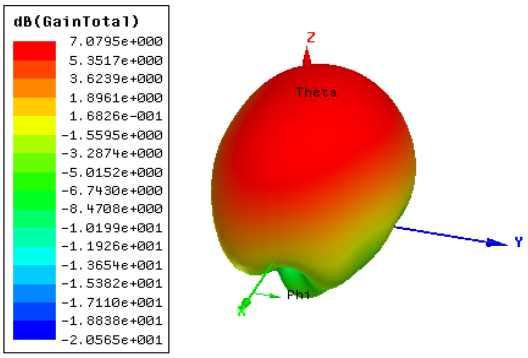

Fig 4.b: 3-D Gainof Model 1 Antenna

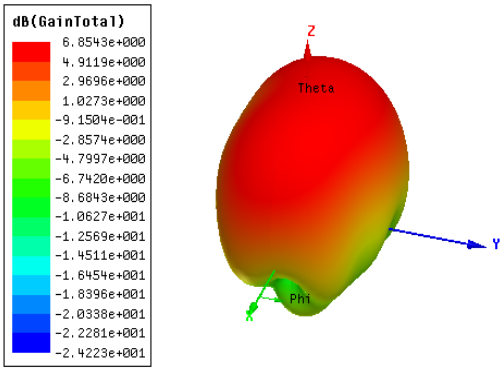

Fig 5.b: 3-D Gain of Model 2 Antenna

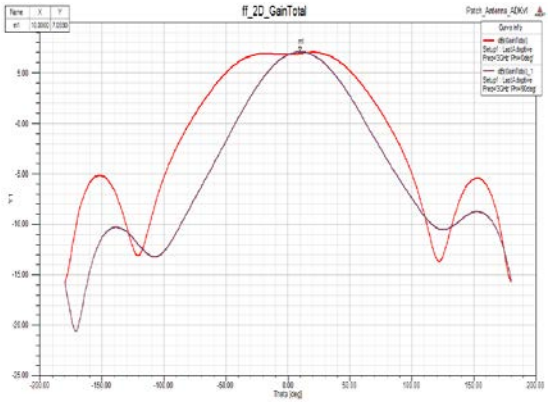

Fig 4.c: 2-D Gain of Model 1 Antenna

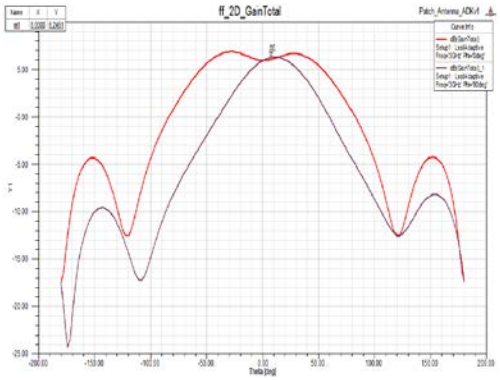

Fig 5.c: 2-D Gain of Model 2 Antenna

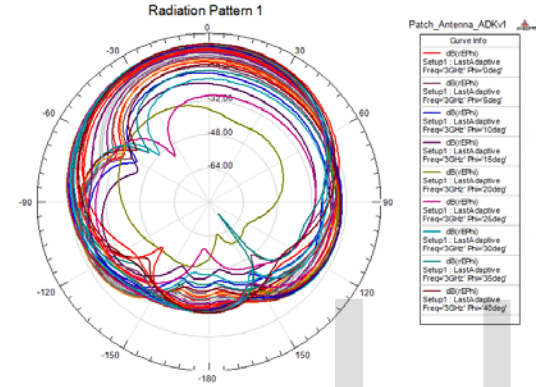

Fig 4.d: Radiation Pattern (rEPhi)

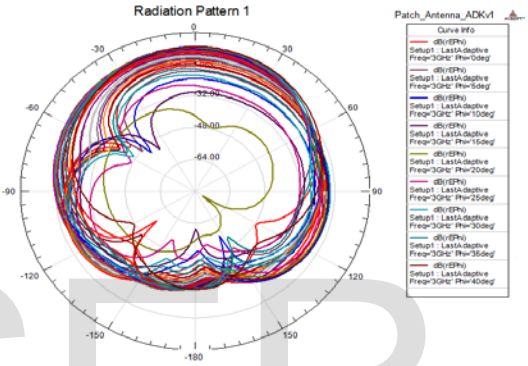

Fig 5.d: Radiation Pattern (rEPhi)

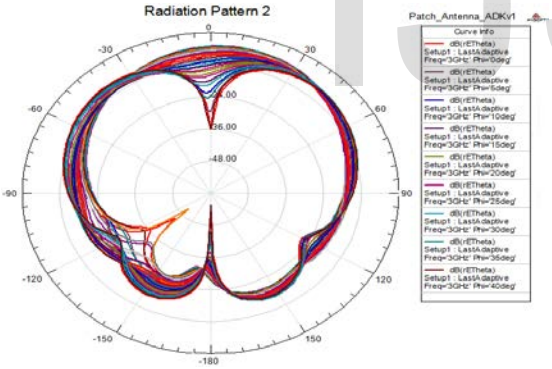

Fig 4.e: Radiation Pattern (rETheta)

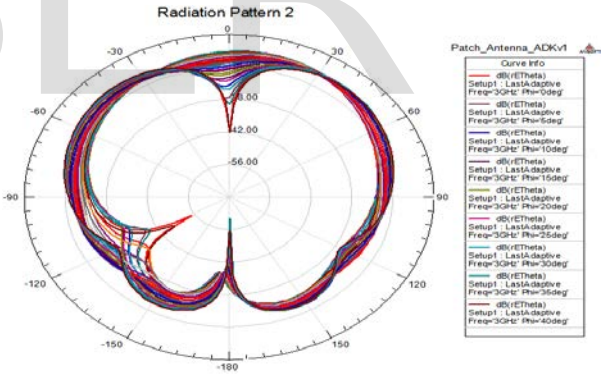

Fig 5.e: Radiation Pattern (rETheta)

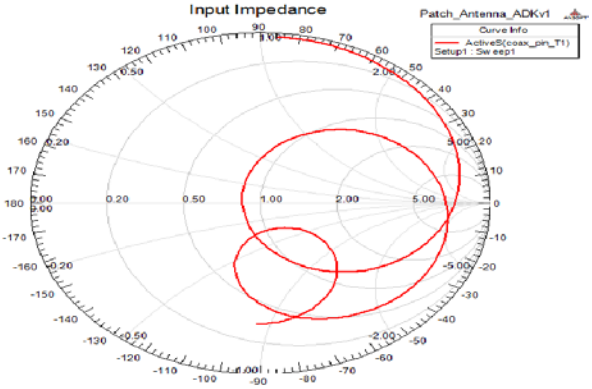

Fig 4.f: Input Impedance smith chart of Model 1 Antenna

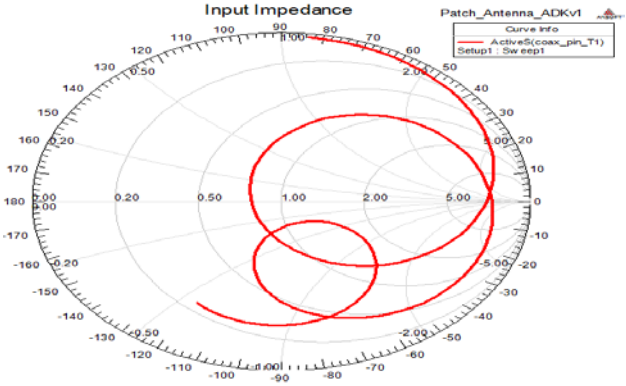

Fig 5.f: Input Impedance smith chart of Model 2 Antenna

Table 4.1: Far Field Radiation Parameters of Model 1 Antenna

S.no	Quantity	Values
1	Max U	0.000454324(W/sr)
2	Peak Directivity	5.14177
3	Peak Gain	5.0321
4	Peak Realized Gain	1.86142
5	Radiated Power	0.00111038(W)
6	Accepted Power	0.00111877(W)
7	Incident Power	0.00306719(w)
8	Radiation Efficiency	0.992501
9	Front to Back Ratio	53.2301
10	Decay Factor	-0

S.no	rE Field	Value	(ɵ, ϕ)
1	Total	0.585286	(0.244346, 0.523599)
2	X	0.323244	(0.558505, 3.14159)
3	Y	0.577031	(0.10472, 1.39626)
4	Z	0.306286	(0.942478, 2.96706)
5	ϕ	0.564847	(0.0349066, 0)
6	ɵ	0.582454	(0.174533, 1.5708)
7	LHCP	0.54969	(0.453786, 3.05433)
8	RHCP	0.554699	(0.453786, 0.0872665)
9	Ludwig3/X dominant	0.399897	(0.698132, 3.05433)
10	Ludwig3/Y dominant	0.582592	(0.174533, 1.48353)

Table 5.1: Far Field Radiation Parameters Model 2 Antenna

S.no	Quantity	Values
1	Max U	0.000316293(W/sr)
2	Peak Directivity	4.90601
3	Peak Gain	4.85382
4	Peak Realized Gain	1.37096
5	Radiated Power	0.000810179(W)
6	Accepted Power	0.000818892(W)
7	Incident Power	0.00289926(w)
8	Radiation Efficiency	0.98936
9	Front to Back Ratio	13.9736
10	Decay Factor	-0

S.no	rE Field	Value	(ɵ, ϕ)
1	Total	0.488349	(0.488692, 3.05433)
2	X	0.30823	(0.558505, 0)
3	Y	0.452253	(0.139626, 1.74533)
4	Z	0.28994	(0.977384, 2.96706)
5	ϕ	0.439991	(0.0349066, 3.14159)
6	ɵ	0.457467	(0.174533, 1.5708)
7	LHCP	0.477949	(0.488692, 3.14159)
8	RHCP	0.467732	(0.488692, 0)
9	Ludwig3/X dominant	0.379495	(0.698132, .0872665)
10	Ludwig3/Y dominant	0.457751	(0.174533, 1.65806)

CONCLUSIONS:

By comparing the various parameters of the two antenna models with different serrations (fig.3.a & fig.3.b), it is concluded that both are having reasonably good return losses, gains and radiation fields. It is also observed that each model is possible to use in two different applications operated in **S** band frequency range. Even though the variable convex serrated MSP antennas radiation field strengths are less than the hybrid triangulated MSP antenna, its return loss, gain and radiation intensities are reasonably sufficient and it also resonated at different frequencies used for different applications.

ACKNOWLEDGMENTS

The Authors would like to express their gratitude to the management of K L University and management of JNTU, Kakinada for their support and encouragement during this work.

REFERENCES:

[1]. Kai Fong Lee, Kwai Man Luk, "Microstrip Patch Antennas ", Imperial College Press, 2011.

[2]. Ramesh Garg, Prakash Bhartia, "Microstrip Antenna Design Hand Book", Artech house, London, 2001.

[3]. J.H.Lu, "Single feed dual-frequency rectangular Microstrip antenna with pair of step-slots", Electron Lett.35, 354-355, March 4, 1999.

[4]. J.S.Hollis,T .J.Lyon, L.Clayton," Microwave Antenna measurements", Scientific Atlanta Inc., Atlanta, USA,Nov.1985.

[5]. ANS/IEEE Standard Test Proccedures for Antenna, ANSI/IEEE Std. 149-1979, IEEE, Newyork, John Wiley Distributors.

[6]. Mustapha Iftissane, Seddik Bri, Lahbid Zenkouar, Ahmed Mamouni, "Conception of Patch Antenna at Wide Band", Int.Journal of Emerg.Sciences, 1(3), 400-417, Sep'2011, Issn:2222-4254

[7]. C. Johnson and Doren Hess,"Conceptual Analysis of Measurements on Compact Ranges", Antenna Applications Symposium, Sep'1979.

[8]. G Srivatsun, Subha Vani," A Compact Multiband Fractal Cantor Antenna for Wireless Applications", European Journal of Scientific Research, pp.273-282, vol.71, No.2, 2012.